Microtubule curvatures under perpendicular electric forces reveal a low persistence length

M. G. L. van den Heuvel, M. P. de Graaff, and C. Dekker*

Kavli Institute of Nanoscience, Section Molecular Biophysics, Delft University of Technology, Lorentzweg 1, 2628 CJ Delft, The Netherlands

Edited by Robert H. Austin, Princeton University, Princeton, NJ, and approved December 31, 2007 (received for review May 4, 2007)

The mechanics of microtubules, cylindrical protein filaments that constitute the cytoskeleton, have been well characterized on long length scales. Here, we investigate the persistence length of short (≈0.1 μm) ends of microtubules by measuring the trajectories of kinesin-propelled microtubules under perpendicular electric forces. We relate the measured trajectory curvatures to the biased thermal fluctuations of the leading microtubule end, and upon including all electrohydrodynamic forces, we find that the persistence length of the microtubule ends is only 0.08 ± 0.02 mm. This is significantly shorter than the well established value of ≈4–8 mm that is measured for long microtubules. Our data are in good agreement with recent theoretical predictions that microtubules mechanically behave as a loose assembly of independent protofilaments on these short length scales.

Microtubules are stiff cylindrical protein filaments that constitute an important part of the cytoskeleton of eukaryotic cells. They have an outer diameter of ≈25 nm and lengths of several micrometers and can serve as tracks that guide the motion of motor proteins such as kinesin. Microtubules are important for defining morphology and providing mechanical stiffness to cells. The mechanical properties of microtubules have therefore been studied intensively for over a decade (1–7). The consensus was that microtubules can be characterized by a persistence length of 4–8 mm (1, 6). However, recent experiments have shown a strongly reduced persistence length for short microtubules, which has been attributed to non-negligible shear deflections on short length scales (4, 7). Most prominently, thermal fluctuations of taxol-stabilized microtubule ends indicated that the persistence length decreased from 5 to 0.11 mm upon decreasing the contour length from 48 μm down to 3 μm (7).

These results have recently been explained by explicitly considering microtubules as assemblies of protofilaments that have compliance due to stretching deformations, but also due to shear displacements of adjacent protofilaments (8, 9). From this picture of microtubules as bundles of wormlike chains, it emerges that microtubules have a bending stiffness that derives from an interplay between the high stiffness of the individual filaments and their soft relative sliding motion. An important consequence of this model is that the persistence length of microtubules depends on their length. For long microtubules, the bending deformation is described by a so-called fully coupled regime, in which the bundle behaves as a homogenous structure with little protofilament sliding. At intermediate deformation lengths, shear deformations dominate the flexibility and lead to a reduction in the persistence length with decreasing microtubule length. At the shortest length scales, microtubules mechanically behave as decoupled assemblies of individual protofilaments, with negligible shear displacements. A prediction from this model is that microtubules shorter than 3 μm are in this decoupled regime, and that the persistence length should approach a limiting value of ≈0.2–0.5 mm (9). A decrease in persistence length with microtubule length down to 3 μm has been measured (7), but shorter length scales were not easily accessible using the same method, and thus the predicted lower limit on the persistence length was not measured.

To measure the persistence lengths of microtubule ends on even shorter length scales, we study the trajectories of kinesin-propelled microtubules subjected to perpendicular electric forces. The (macroscopic) curvature of the microtubule trajectories is an amplification of the microscopic bending of the ≈0.1-μm short ends of microtubules in our experiments and provides a convenient measure of their stiffness. We find a value that is significantly lower than measured for entire microtubules, but that is two orders of magnitude higher than expected from extrapolating the previously reported decrease in stiffness (7) to our length scales. Our data suggest a lower limit on the persistence length of very short microtubule ends that is in excellent agreement with the recently proposed mechanics of wormlike bundles (8, 9). Additionally, our measurements provide a quantitative understanding of the steering mechanism of microtubules in bionanotechnological applications (10), which can help a rational design of structures for kinesin-powered devices.

Electric forces in microfabricated structures have earlier proven to be a versatile tool for the manipulation and study of biomolecules. For example, electrokinetic forces have been used to suppress Brownian motion and trap individual proteins for optical observation (11), to probe force–velocity diagrams of myosin-driven actin filaments (12), and to study binding kinetics of microtubules onto kinesin-coated surfaces (13). Electric forces are advantageous because they can exert a homogeneous force density of well controlled magnitude and direction on biomolecules, which are naturally charged. In contrast, optical tweezers apply a localized force and require linkage of the molecule to a bead where the exact geometry of the linkage is often unknown. Hydrodynamic shear flows require knowledge of the detailed shear profile, and thermal forces are hard to control. We perform our experiments in micronsized channels because their large surface-to-volume ratio prevents Joule heating of the solution while the electric field is applied. Consequently, we can apply much higher electric fields than in regular flow cells (14).

Results and Discussion

The experimental layout of our devices is depicted in Fig. 1. Channel structures were etched 1 μm deep in fused-silica substrates between entrance reservoirs separated by 5 mm and subsequently bonded using another fused-silica substrate (Fig. 1 *a* and *c*). We reconstituted kinesin-driven microtubule motility in the channels using pressure-driven flows to flush the protein constituents (casein, kinesin, microtubules) from one of the entrance reservoirs through the channels. Motility of taxol-stabilized microtubules (polymerized for 45 min at 37°C) was observed using fluorescence microscopy through the fused silica. Electric fields were induced in the channels by application of a DC-voltage difference between platinum electrodes in the reservoirs, under constant monitoring of the current (Fig. 1*b*).

To study microtubule trajectories under perpendicular electric fields, we fabricated channels with a perpendicular crossing (Fig. 1 *d* and *e*). The narrow channel (vertical channel at the bottom of the figure) serves to feed microtubules into the wide horizontal channel in which a homogeneous electric field is present. In Fig. 1*d*, we show representative fluorescence images of microtubules that move while an electric field is continuously applied. We highlighted three

Author contributions: M.G.L.v.d.H. and C.D. designed research; M.G.L.v.d.H. and M.P.d.G. performed research; M.G.L.v.d.H. and M.P.d.G. analyzed data; and M.G.L.v.d.H. and C.D. wrote the paper.

The authors declare no conflict of interest.

This article is a PNAS Direct Submission.

*To whom correspondence should be addressed. E-mail: c.dekker@tudelft.nl.

This article contains supporting information online at www.pnas.org/cgi/content/full/0704169105/DC1.

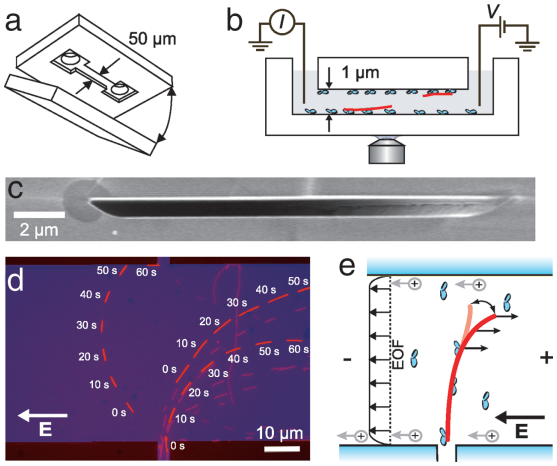

Fig. 1. Experimental layout. (*a*) Microchannels were fabricated by bonding two fused-silica substrates. One substrate contained etched channels between 1-mm-diameter entrance holes. (*b*) Schematic of the device. Electric fields were induced by applying a voltage difference to platinum electrodes in the reservoirs, separated by 5 mm, while monitoring the current. (*c*) Scanning-electron microscope image of a cross-section of a channel. (*d*) Overlay of fluorescence images (with 10-s intervals) of microtubules subjected to a homogeneous electric field ($E = 26$ kV/m) that is applied in the 50-μm-wide channel. Microtubules enter the structure from the vertical channel below. Three microtubules are highlighted for clarity. (*e*) Illustration of the curvature experiment. Thermal fluctuations of the free tip of a microtubule are biased by the force resulting from the electric force and electro-osmotic flow (EOF).

microtubules that enter from the small channel, in snapshots taken with 10-s intervals. All three microtubules traverse the structure with a pronounced curvature of their paths, in such a way as to become aligned against the field.

The electric field induces a constant force density on the homogeneously charged microtubule in the direction opposite to the electric field. Kinesin molecules, distributed along the length of the microtubule, exert the opposing forces and prevent the movement of the microtubule perpendicular to its axis. As was suggested and demonstrated previously (10, 12, 14, 15), the thermally fluctuating tip of the microtubule is biased into the direction of the force (Fig. 1*e*), thereby orienting the microtubule slowly, in a step-by-step fashion, into the direction of the electric field.

For a quantitative determination of the curvature of microtubule trajectories, we acquire fluorescence images with 1-s intervals of a large number of microtubules entering the electric field region. We used custom-written MATLAB routines to trace the coordinates of the leading and trailing ends of all microtubules that traversed the structure during 15 min. In Fig. 2*a*, we show microtubule trajectories that were measured under an electric field of 18 kV/m. For later analysis, we excluded those parts of the trajectories that have touched one of the channel walls. As expected, most of the trajectories originate from the small injection channel below and display a pronounced bending to the right. Some trajectories originate from microtubules that were already present in the wide channel, and these trajectories also tend to align with the field. There is a large variance in the orientation with which microtubules enter the channel, and the magnitude of the perpendicular force decreases upon aligning with the field, thereby reducing the curvature (10).

In Fig. 2*b*, we show a selection of paths under two different fields. The green and red trajectories are from microtubules that originate from the injection channel and that are being subjected to electric fields of 8.8 kV/m and 35 kV/m, respectively. It is clear that the bending of microtubule trajectories becomes more pronounced when we increase the electric field strength. Note that the spread between individual paths under a single electric field is of the same order as the differences between trajectories under different electric fields.

To unambiguously show that the microtubules indeed align with the electric field by a bending of the leading tip, we display the coordinates of both leading and trailing ends of two microtubules in Fig. 2*c*. At both electric fields, even at the highest field strength used ($E = 44$kV/m), the coordinates of the front and rear ends of the microtubule overlap perfectly over the entire trajectory. This demonstrates that, within the resolution of our measurement, both ends of the microtubule trace the same path. In other words, they get propelled by the same kinesin molecules and there is no motion of the microtubule perpendicular to its long axis. The field-induced alignment of the microtubule must therefore be attributed to bending of the leading tip.

We now relate the macroscopically observable curvature of the trajectory to the microscopic properties of the microtubule tip. The microtubule is propelled by several bound kinesin molecules that are distributed stochastically along its length with average spacing $\langle d \rangle$. Upon progression of the microtubule, the leading tip will progressively increase in length from 0 to a value d, just before the moment of binding to the next kinesin molecule. In the absence of any forces, the tip will fluctuate under thermal forces, with a mean change in orientation of the tip $\langle \theta'_{\mathrm{m}} \rangle = 0$. However, an externally applied force $f_{\perp}$ that is oriented perpendicular to the microtubule displaces the equilibrium position of the free tip (Fig. 2*c*). To calculate the force-induced change in orientation of the leading tip, we assume that the microtubule is clamped at the foremost kinesin molecule. At the moment of attachment to the next motor, the increase in orientation of the tip, θ'_{m}, can then be calculated as [supporting information (SI) *Appendix*]

$$\theta'_{\mathrm{m}} = \frac{d^3}{6k_{\mathrm{b}}Tp} f_{\perp}, \qquad [1]$$

where k_{b} is Boltzmann's constant, T temperature, and p the persistence length of the microtubule tip.

We describe the microtubule trajectory using (macroscopic) coordinates θ and s, as defined in Fig. 2*c*. Because the trajectory of the microtubule is determined by the orientation of its leading end

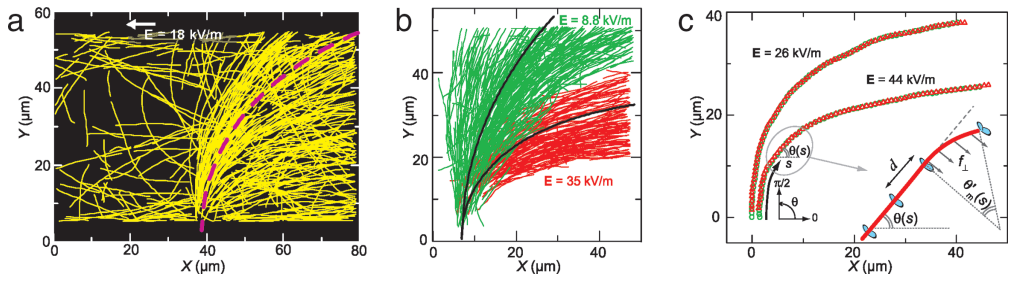

Fig. 2. Measurements of microtubule trajectories. (*a*) Microtubule trajectories under an electric field $E = 18$ kV/m. All trajectories acquired during a 15-min measurement are shown. The dashed line shows the average trajectory that we infer from analysis of the curvature (Eq. **11** in *SI Text*). (*b*) Selection of trajectories at two different field strengths. At the highest electric field (red) the curvature is clearly more pronounced and the alignment is faster. (*c*) Overlapping coordinates of leading (red triangles) and trailing (green circles) ends of two different microtubules under different electric fields show that there is no motion perpendicular to the microtubule axis. The orientation θ'_{m} of the leading tip of the microtubule, just before attachment to the next kinesin motor, determines the trajectory curvature $\frac{d\theta}{ds}$ at any point s along the trajectory.

and consists of the average of many small increments we assert that $\left\langle \frac{d\theta}{ds}(s) \right\rangle = \left\langle \frac{\theta'_m(s)}{d} \right\rangle$, which holds as long as the curvature is measured on length scales larger than $\langle d \rangle$. Substituting $f_\perp = f_e \sin\theta$ in Eq. **1**, yields for the trajectory curvature

$$\left\langle \frac{d\theta}{ds} \right\rangle = \frac{\langle d \rangle^2}{3k_bTp} f_e \sin\theta, \qquad [2]$$

where f_e is the electric field-induced force. In this equation, we performed the averaging over an exponential distribution of tip lengths d. The rationale for this is that the binding of the progressing microtubule tip to a new kinesin motor is a Poisson process and, consequently, values of d are exponentially distributed with mean $\langle d \rangle$, with $\langle d^2 \rangle = 2\langle d \rangle^2$.

This description of the trajectory, which employs the angular deviation of the tip, is more appropriate than the modeling in terms of the spatial deflection of the tip, which was previously employed (10, 16). It does not rely on the small-angle approximation, and it naturally captures the reduction of the perpendicular force upon alignment with the electric field. In its derivation we assumed that the kinesin molecules have no compliance, and that the microtubule tip is fixed at the frontmost motor. We further discuss the limitations of this assumption below.

We determine experimental tangent angles θ and curvatures $\frac{d\theta}{ds}$ from the measured microtubule trajectories at every coordinate. In this way, we obtain a large number of orientation-dependent curvatures. Fig. 3*a* displays measured trajectory curvatures as a function of tangent trajectory angle at $E = 18$ kV/m. We confirm that curvature has a sinusoidal dependence on orientation, as expected from Eq. **2**. Given the layout of our device, most trajectories start at $\theta = \pi/2$, and end at $\theta = 0$ and, consequently, the error bars are smallest in this range.

In order to eliminate the orientation dependence in our quantitative analysis, we divide the measured curvatures by the sine of the tangent angle (Eq. **2**). The resulting orientation-invariant curvatures $\frac{d\theta}{ds}(\sin\theta)^{-1}$ are plotted in Fig. 3*b* versus θ. We find that there is a strong divergence in the curvature around $\theta = 0, \pm\pi$, which are those parts of the trajectories that are aligned with the electric field. In particular for these orientations we expect no appreciable influence of the electric field. The observed divergence is due to the division of finite, thermally driven, trajectory curvatures by very small ($\approx$0) values of $\sin\theta$. For the determination of the field-induced curvature, we thus retain only data points for orientations where $|\sin(\theta)| \geq 0.5$, that is, those parts of the trajectories where there is an appreciable field-induced curvature (indicated between red lines in Fig. 3*b*).

The histogram in Fig. 3*c* displays the resulting distribution of measured orientation-invariant curvatures. We observe that the shape of the distribution is Gaussian, which we attribute to thermal fluctuations. Indeed, the orientation of the end of a one-sided clamped beam with length $\langle d \rangle$ is expected be Gaussian distributed with a standard deviation $\sigma = \sqrt{\langle d \rangle / p}$ (17).

We take the center of a Gaussian fit (red line in Fig. 3*c*) as a measure of the mean orientation-invariant curvature at this particular field. We measured the orientation-invariant curvatures for a range of electric fields from 0 to 44 kV/m and Fig. 3*d* displays the results as a function of the electric field. The error bars denote errors in the mean of the distribution centers, not the standard deviation of each individual distribution which is much larger. As expected (Eq. **2** and $f_e \propto E$), the orientation-invariant curvature increases linearly with the electric field with a slope of 1.30 ± 0.02 V^{-1}. We note that retaining only points of $|\sin(\theta) \geq 0.5|$ has no significant effect on this value (data not shown).

To determine the persistence length of the microtubule tip, we need to calibrate the magnitude of the electric field-induced force that we apply. The magnitude of this force in the experimental situation of so-called stationary electrophoresis equals (18)

$$f_\perp = c_\perp \mu_{\perp,e} E_\perp, \qquad [3]$$

where $\mu_{\perp,e}$ is the mobility of a freely suspended microtubule inside the channel during free electrophoresis, and $c_\perp$ is the perpendicular Stokes drag coefficient per unit length of a microtubule tethered

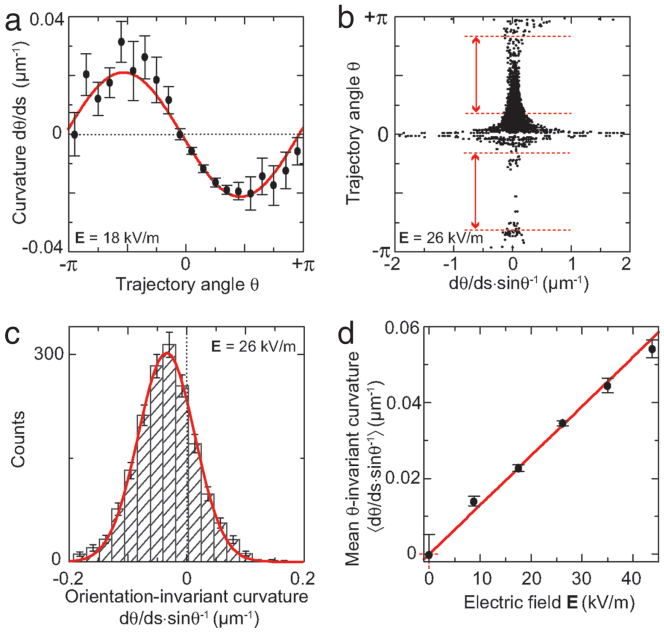

Fig. 3. Quantification of microtubule-trajectory curvatures. (*a*) Measured trajectory curvature as a function of tangent trajectory angle. We show binned values [mean ± standard error of the mean (SEM)] of 3,600 measurements. (*b*) Orientation-invariant curvatures for different θ. The divergence around $\theta = 0$ and $\pm\pi$ arises from division by small values of $\sin(\theta)$. The intervals denoted between the red lines ($|\sin(\theta)| > 0.5$) are included in the histogram. (*c*) Histogram and Gaussian fit of orientation-invariant trajectory curvatures of the data in *b*. (*d*) Mean orientation-invariant curvature, as determined from Gaussian fits to histograms, as a function of electric field. Error bars denote the error in the fit.

to the surface via kinesin molecules. We emphasize that this result for calculating the magnitude of the electric-field induced force is remarkably simple and exact, given the complicated boundary conditions due to the nearby walls. This simplicity stems from the linearity of the Navier–Stokes equations that allows to split the problem of stationary electrophoresis into two different problems with known solutions, being free electrophoretic motion and purely hydrodynamic motion of a microtubule close to a surface. We show this formally in the Supporting Information.

The perpendicular hydrodynamic drag-coefficient $c_\perp$ (Eq. **3**) for a microtubule tethered to kinesin on a casein-coated surface was measured as $c_\perp = 1.19 \pm 0.11 \times 10^{-2}$ Ns/m^2 by Hunt *et al.* (19). This was done by observing the rotational diffusion of microtubules tethered to a single kinesin molecule. This value of the drag-coefficient corresponds to an elevation of the microtubule axis of 18 ± 1 nm above the casein surface, in good agreement with a direct measurement of this distance (20). The value of $\mu_{\perp,e}$ in Eq. **3** was measured by electrophoresis of freely suspended microtubules in our channels (as described in ref. 21), which yields $\mu_{\perp,e} = -(1.03 \pm 0.01) \times 10^{-8}$ m^2/Vs. From Eq. **3**, we thus calculate that in our experiments we have applied force densities up to a maximum $f_e = 5.4 \pm 0.6$ pN/μm at the highest electric field of 44 kV/m. With this knowledge, we determine from the slope in Fig. 3*d* that $\frac{\langle d \rangle^2}{p} = 1.30 \pm 0.16 \times 10^{-10}$ m (Eq. **2**).

We can obtain an estimate of the average distance between bound kinesin molecules $\langle d \rangle$ from observations of the movement of very short microtubules in the absence of applied forces. Long microtubules are bound to and propelled by several kinesin molecules distributed along their length and will therefore preserve their directionality. However, if the microtubule length becomes small and comparable to $\langle d \rangle$, then occasionally the filament will be bound to only a single kinesin molecule and display diffusive rotational motion around the motor (19, 22), thereby rapidly changing its orientation. The average distance traveled by the microtubule between successive rotations, $\langle S \rangle$, is strongly dependent on the ratio of the microtubule length L and the average tip length $\langle d \rangle$.

Duke *et al.* (22) analytically determined the average distance $\langle S \rangle$ between points where a microtubule is bound to only a single kinesin motor by considering the stochastic evolution of the number of motors that are bound to a filament. They derived (equation 4 in ref. 22) that

$$\langle S \rangle = \frac{L + 2\langle d \rangle}{L + 3\langle d \rangle} \frac{\langle d \rangle^2}{L} \left(e^{L/\langle d \rangle} - 1 - \frac{L}{\langle d \rangle} \right). \quad [4]$$

Thus, a measurement of $\langle S \rangle$ for a microtubule of known length L can provide a measurement of the average tip length $\langle d \rangle$.

To illustrate this method, we show in Fig. 4*a* traces of two short microtubules that move in markedly different manners. The longer microtubule of the two (black trace in Fig. 4*a*, fluorescence image in Fig. 4*c*) moves, as expected, in a smooth fashion over the surface without sudden changes of direction. In contrast, the shorter microtubule of the two (red trace in Fig. 4*a*, fluorescence image in Fig. 4*d*) moves much more irregularly, with many sharp turns in its trajectory. Given the sudden changes in direction, this shorter microtubule is, on several occasions in its trajectory, bound to only a single kinesin motor.

We quantify this by plotting the trajectory curvature $d\theta/ds$ as a function of the trajectory distance s for the two trajectories (Fig. 4*b*). The longer microtubule has a trajectory curvature that never exceeds 0.6 μm^{-1} along its 50-μm-long trajectory (black trace). The shorter microtubule has a curvature that is sharply peaked at several points along its 100-μm-long trajectory (red trace), presumably because at these points the filament is bound to only a single motor. Depending on the magnitude of the curvature that one requires to qualify a turning point as free pivoting motion, one can identify 10–17 of these pivoting points along the trajectory. From this we calculate that $\langle S \rangle = 6 - 10$ μm. Although we cannot determine $\langle S \rangle$ with a great accuracy, we will show below that it nevertheless allows for a rather accurate estimate of $\langle d \rangle$.

To calculate $\langle d \rangle$ from Eq. **4**, we determine the lengths of short microtubules from a deconvolution of intensity line scans along their long axes. For the shortest microtubule (shown in Fig. 4*d*) we show the intensity profile along its length in Fig. 4*f*. Due to the finite optical resolution of the microscope, the profile consists of a convolution of the objectives point-spread-function (PSF) with the microtubule length and, as a result, its length is overestimated. We approximate the PSF from the intensity profile perpendicular to the microtubule axis (Fig. 4*e*). This profile has a full-width-at-half-maximum (FWHM) of 0.35 μm, which is much more than the 25-nm microtubule diameter, justifying its use as an approximation of the PSF. Deconvolution of the intensity length profile shown in Fig. 4*f* yields a value for the length of the shortest microtubule of 0.62 μm. We repeated this analysis on the same microtubule in different images to get an estimate of the error in the determination of the length and we found that $L = 0.63 \pm 0.05$ μm [mean $\pm$ standard deviation (STD) as determined from nine different images].

We now determine the average tip length $\langle d \rangle$ using Eq. **4**. In Fig. 4*g*, we plot $\langle S \rangle$ as a function of $\langle d \rangle$ for a microtubule of length $L = 0.63 \pm 0.05$ μm (red line). For a microtubule of this particular length, we determined that $\langle S \rangle = 6$–10 μm (Fig. 4*b*), which corresponds to an average tip length $\langle d \rangle = 0.10 \pm 0.02$ μm (Fig. 4*g*). The error in this value includes the error in $\langle S \rangle$, but more importantly also the error in the determination of the microtubule length (indicated by the red dotted lines in Fig. 4*g*).

The value that we determine for $\langle d \rangle$ is consistent with the observation that a slightly longer microtubule (shown in Fig. 4*c*, black trajectory in Fig. 4*a*) has a trajectory without pivoting. For this microtubule of length 0.89 ± 0.06 μm, which is only a factor 1.4 longer, Eq. **4** predicts that $\langle S \rangle$ is in the range of 40–230 μm (black line in Fig. 4*g*). Also note that the markedly different trajectories shown in Fig. 4*a* are only consistent with a very small range of possible $\langle d \rangle$. If $\langle d \rangle$ were a factor of two larger, both microtubules would show very erratic movement, whereas if $\langle d \rangle$ were a factor of two smaller, both microtubules would move in smooth trajectories.

We find that the forces that are exerted on the leading tip are small compared to typical forces that can be withstood by a kinesin motor. At the highest electric field, the force on the tip amounts to only 0.5 ± 0.2 pN. This force will yield an average deflection of the microtubule end

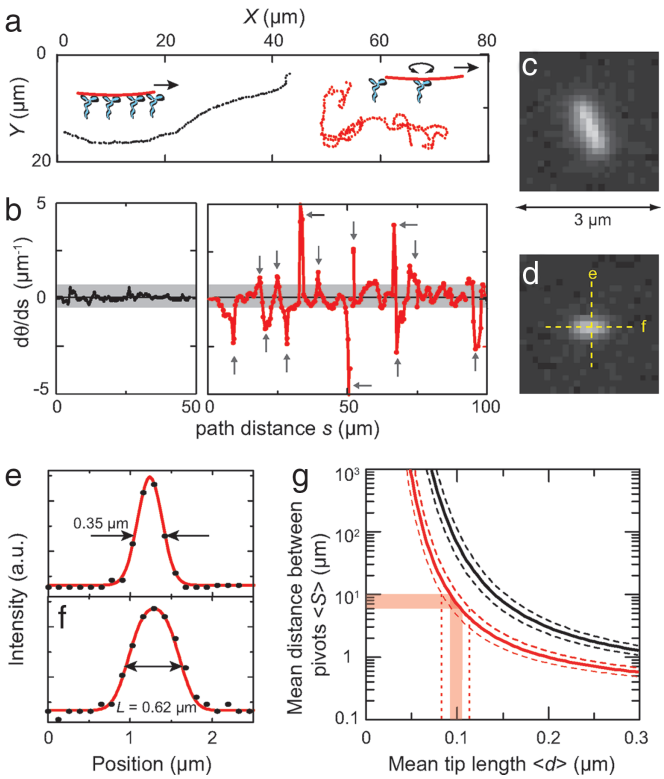

Fig. 4. Measurement of microtubule tip length. (*a*) Trajectories of two short microtubules without an applied electric field. One microtubule (shown in *c*, with length 0.89 ± 0.06 μm) moves without sudden changes of direction (black trace). The shorter microtubule (shown in *d* with length 0.63 ± 0.05 μm) displays sudden changes in direction (red trace), presumably because at these moments it is bound to only a single kinesin molecule and rotationally free. (*b*) Curvature as a function of distance along the trajectory for the two trajectories shown in *a*. (*c* and *d*) Fluorescence images of the two microtubules. Intensity line-scans parallel and perpendicular to the shortest microtubule are denoted. (*e* and *f*) Intensity linescans taken along the directions indicated in *d*. The scan perpendicular to the microtubule (*e*) is used as an approximation of the point-spread-function, with the full-width-at-half-maximum indicated. In the scans along the microtubule (*f*), we indicate the deconvoluted length. (*g*) Plots of Eq. **4** for microtubules of lengths 0.63 ± 0.05 μm (red lines) and 0.89 ± 0.06 μm (black lines). The dotted lines indicate the margins in $\langle S \rangle$ due to the error in L.

of less than a nanometer, which is much smaller than its 25-nm radius. It is remarkable that a succession of these small deviations can lead to a complete reorientation of the entire microtubule. Interestingly, the field-induced bending energies are thus smaller than $k_b T$. This is also apparent from the fact that the thermally induced variance in the measured curvatures (Fig. 3*c*) exceeds the field-induced deviation of the mean curvature from zero. We can thus safely assume that the value that we determined for the tip length under unloaded conditions also applies in the situation when a perpendicular force is applied. Any possible effect of pulling the microtubule tip loose from the leading kinesin motors would be expected to increase with force and consequently, the measured curvature would increase more than linearly with the electric field. The fact that, instead, curvature is linearly proportional to E over the entire range of fields (Fig. 3*d*) shows that the measured value of $\langle d \rangle$ applies at all the forces that we have probed.

With our estimate for the average inter-kinesin distance, we are able to determine the persistence length of the leading microtubule end as $p = 0.08 \pm 0.02$ mm. Importantly, this number is much lower than the 4–8 mm bulk value for long microtubules (1, 6). Moreover, it places an important lower limit on a recently measured decrease in persistence length with a reduction in microtubule length (7). Both observations are discussed at greater length below.

First we note that the 0.08-mm value depends on the assumptions in the modeling of the bending of the leading end of the microtubule,

in particular on the assumption that the microtubule tip is clamped at its base at the frontmost kinesin molecule. In reality, the kinesins have a finite compliance which may allow additional bending of the microtubule further down along its length, leading to an underestimation of the persistence length using our model. The strength of such an effect depends strongly on values of a number of parameters that are not accurately known, such as the kinesin compliance, the stiffness of the microtubule, and the distribution of kinesins along the microtubule. A proper calculation to estimate the magnitude of this effect requires stochastic simulations that take into account the random placements of motors on a surface, the nonlinear compliance for kinesin (a combination of limited rotational freedom of the (reduced) stalk, and its stretching compliance), and averaging over a large number of deflection events, but this is beyond the scope of the current work.

As a control measurement, we verified the reduced sub-mm persistence length of our microtubule ends by an independent method, i.e. from observing the stochastic trajectories of microtubules over kinesin-coated surfaces in the absence of any (electrical) forces (23), according to the method proposed by Duke *et al.* (22). The time-dependent variance of the tangent–trajectory angle provides a measurement of the persistence length of the leading microtubule end and is independent of the length of the kinesin tip. In these experiments (23) we found that the persistence length of the microtubule ends was 0.24 ± 0.03 mm, again much lower than the $\approx$5 mm for long microtubules. Other reported values of the persistence length of microtubule trajectories range from 0.1 mm (24) to 0.5 mm (25), which also agree well with the value that we determine. The lower value of the tip persistence length as determined from our electrical curvature experiments may be attributed to the kinesin compliance, as discussed above.

In a second control measurement, we verified that the persistence length for long microtubules is indeed in the mm range under our experimental conditions. To this end we analyzed the thermal fluctuations of microtubules with lengths between 22 and 40 μm following the method of ref. 1. The results of this analysis are presented in Fig. 8 of *SI Appendix*. From the analysis of the variance of up to the first three modes of seven different microtubules, we obtain a persistence length of 3.6 ± 0.3 mm. This value is likely a lower bound, since even a slight degree of rotational freedom around its long axis of a microtubule that is not perfectly straight will contribute to the measured variance and thus lead to an underestimate for the measured persistence length (*SI Appendix*). We therefore conclude that the persistence length of our microtubule ends is indeed at least one order of magnitude lower than the persistence length of our microtubules when they are probed on a long length scale.

A reduction in the persistence length for shorter microtubules was also reported in two other works (4, 7). First, Kis *et al.* (4) used an atomic force microscope (AFM) to induce elastic deformations on gluteraldehyde-stabilized microtubules that were suspended over 0.08- to 0.17-μm gaps. They found that the persistence length decreased from 0.11 to 0.02 mm in this size range. These results cannot straightforwardly be compared to ours, because in the AFM experiments the microtubules were supported at both ends, which increases the relative contribution of shear-induced deformations (see below) and will result in a enhanced compliance to bending. The gluteraldehyde cross-linker used for stabilization further complicates the comparison. Note that the suspended deformation length is the relevant length scale and not the microtubule contour length.

Second, more recent measurements by Pampaloni *et al.* (7) reported a systematic decrease in the persistence length of taxol-stabilized microtubule ends from 5.0 mm to 0.11 mm when the microtubule length decreased from 48 μm to 2.6 μm. They attributed this effect to the strongly anisotropic material properties of microtubules (4, 7), which are hollow, cylindrical structures that are built from 13 protofilaments, arranged in parallel. Both refs. 4 and 7 argue that the deflection of the microtubule consists of both bending and shear deformations, where the shear deformations arise mainly due to sub-nanometer displacements of adjacent protofilaments. The deflection of a microtubule over length L scales $\propto L^3$ for pure bending, but $\propto L$ for shear deformations and the latter thus becomes dominant for short L. This model predicts a persistence length that decreases $\propto L^{-2}$ for short microtubules, which describes the data of Pampaloni *et al.* well in their length range of 2.6–48 μm.

However, an open question remained what will happen with the persistence length for microtubule bending on even shorter length scales, below 2.6 μm. The $\propto L^{-2}$ model in Pampaloni *et al.* predicts a vanishing persistence length when the microtubule length approaches zero. In contrast, a recently proposed theoretical model that describes bending of microtubules by considering them as a bundle of wormlike chains (8, 9) (in which the N protofilaments constitute the individual bundle components) predicts a saturation of the persistence length upon decreasing the microtubule length. The worm-like bundles display a so-called state-dependent bending stiffness that derives from the interplay between the bending stiffness of the individual constituting protofilaments (with persistence length p_0) and sliding motions of the filaments, governed by the shear modulus of microtubules that originates from extensible inter-protofilament contacts.

A consequence of the state-dependent bending stiffness is that three elastic regimes emerge to describe microtubule bending, depending on the deformation length over which microtubule bending occurs (9). For long deformation lengths, the bending is described as a fully coupled regime in which the bundle of protofilaments behaves as a homogenous structure, in which shear deformations are negligible. The resulting persistence length of the microtubule (p_{bulk}) is proportional to the square of the number of constituting protofilaments ($p_{\text{bulk}} = N^2 p_0$). For intermediate deformation lengths, the bending stiffness of the microtubule is described as a shear-dominated regime, in which shear deformations in the microtubule cause a reduction of the persistence length with decreasing deformation length ($\propto L^{-2}$). These two regimes have been used to describe the data of Pampaloni *et al*. (7). However, in this picture a third decoupled regime emerges for very short deformation lengths, in which the individual protofilaments bend independently like sheets in a loose stack of paper (8, 9). In this case, the resulting bending stiffness of the microtubule is simply proportional to the number of protofilaments, $p = Np_0$ (9). This result predicts that microtubules are in the decoupled regime when the deformation length is shorter than $L \approx 3.5$ μm and places a lower limit on the bending rigidity of microtubules of $p_0 \approx p_{\text{bulk}}/N$ (9).

Our experimental data are consistent with the prediction that microtubules are in a decoupled regime at the submicrometer length scale that we probe. The predicted value of the persistence length for decoupled bending is $p_0 \approx 0.3$ mm upon using the value of $p_{\text{bulk}} = 3.6$ mm that we measure and $N = 13$ protofilaments. In contrast, the linear elasticity model (7) predicts 0.0002 mm for microtubules of $\approx$0.1 μm length. From our electrical curvature experiments, we find a tip persistence length of $p = 0.08 \pm 0.02$ mm, which is much larger than the value of 0.0002 mm. As discussed above, this value for the persistence length of the tip represents a lower bound. Indeed, we measured a value of 0.24 ± 0.03 mm (independent of kinesin surface density over one order of magnitude) from observation of stochastic microtubule trajectories over kinesin-coated surfaces (23), which is in good agreement with the predicted value of $p_0 \approx 0.3$ mm. We estimate that in the latter experiments, upon varying the kinesin density, the average microtubule tip-length varies roughly between 0.1–1 μm. Thus, the observed constant value of the persistence length in this range is consistent with the prediction that microtubules are in the decoupled bending regime for deformation lengths smaller than $L \approx 3.5$ μm.

Finally, our results also provide input for bionanotechnological applications, in which kinesin-propelled microtubules can act as shuttles transporting an attached cargo through micro-fabricated devices (26, 27). Our first estimate of the distance $\langle d \rangle$ between bound kinesin molecules serves to determine the surface density σ of active kinesin molecules as $\sigma = 1/\langle d \rangle w$, where $w \approx 20$ nm is the distance over which a kinesin molecule can reach to interact with a microtubule (22). We find that $\sigma \approx 5 \times 10^2$ μm^{-2}. Furthermore, from the analysis of the distribution of trajectory curvatures we inferred that thermal fluctuations are the main cause of the dispersion in microtubule trajectories.

Conclusions

Microfabricated structures are a very useful tool for the study of biomolecules. We have used microfabricated channel structures for

a controlled study of microtubule trajectories under perpendicular electric fields. We have measured the curvature of a large number of microtubule trajectories for different values of the electric field. We related the trajectory curvature to the bending of the microtubule tip, which allows us to infer the stiffness of the microtubule ends. For this purpose, we calibrated the magnitude of the electric field-induced force, and we determined the average length of the leading tip $\langle d \rangle = 0.1 \pm 0.02$ μm from observations of the trajectories of very short microtubules. With this knowledge, we were able to infer that the apparent persistence length of taxol-stabilized microtubule ends is 0.08 ± 0.02 mm.

The low value of the persistence length that we measure for our microtubule ends provides the first measurements on very short taxol-stabilized microtubules. The value of 0.08 ± 0.02 mm that we find for the persistence length is significantly lower than the 4–8 mm values that have been reported for long microtubules. We have verified that the persistence length of 22–40 μm long microtubules under our experimental conditions was indeed much larger (3.6 ± 0.3 mm) than the persistence length of the microtubule ends. Our results supplement recent measurements of reduced persistence lengths for short microtubules on a much shorter length scale. The persistence length of our 0.1 ± 0.02 μm long microtubule ends is significantly higher than the value of 0.0002 mm that is predicted from extrapolating the linear elasticity model in ref. 7.

Our data can be taken as experimental evidence for a lower bound on the persistence length of short lengths of microtubules and are consistent with a recently proposed theory describing the mechanics of wormlike bundles, which predicts a lower limit of the persistence length very short microtubules of ≈0.2 mm. According to this theory, our data demonstrate that microtubules at a length scale of 0.1 ± 0.01 μm are in a decoupled regime and bend as a loose assembly of protofilaments. Furthermore, our results provide a quantitative understanding of the steering mechanism of microtubules on kinesin-coated surfaces, which is of interest for technological applications employing molecular motors (10).

Materials and Methods

Microfluidic channels were fabricated between two 1-mm-diameter entrance holes in 500-μm-thick fused-silica substrates. Substrates were cleaned in acetone, fuming nitric acid (HNO_3), and iso-propanol alcohol (IPA). The substrates were covered with 35 nm chromium (Cr) and 800 nm e-beam-sensitive resist polymethylmethacrylate (PMMA). Channels were defined in the resist with a Leica electron-beam pattern-generator and developed in a mixture (1:3) of methyl-isobutyl ketone and IPA. The remaining Cr layer in the structures was removed by a 1 min immersion in Cr etchant. Channels were wet-etched 1 μm deep into the substrates using ammonium-fluorid etchant. After etching, the remaining resist and Cr were removed using PRS3000 and Cr etchant. Channels were sealed using a silica-bonding procedure (28). Both the channel and sealing substrates were cleaned in PRS3000 and HNO_3. Then, the substrates were dipped into a 0.5% solution of hydrofluoric acid for 1 min. A 2% sodium-silicate solution (Sigma) was spin-coated onto the cover substrate, immediately followed by pressing the sodium-silicate coated surface onto the patterned channel surface. Finally, the devices were cured for 1 h at 90°C.

Channel structures were coated with casein and kinesin using pressure-driven flows (≈5kPa), created by water columns on the entrance reservoirs. First, channels were filled with BRB80 buffer [82 mM Pipes ($pH \sim 6.9$), 1 mM $MgCl_2$, 1 mM EGTA] supplemented with 1 mM adenosine-triphosphate (ATP), 100 μM paclitaxel (Taxol), and 2% 2-mercaptoethanol (BME) and any air bubbles were removed with pressure. Then, 20 μl of 0.9 mg/ml casein solution in BRB80 was added to an emptied reservoir and flushed through the channels for 1.5 h. Finally, a kinesin solution [70 μg/ml his-tagged full-length *Drosophila* conventional kinesin (29), 0.9 mg/ml casein, 9 mM ATP in BRB80] was flushed through the channels with the same pressure for 2 h. Because proteins can enter the structures only from the reservoir, the protein coating progresses from upstream towards downstream with time. In the last step, a motility solution containing microtubules (200 nM tubulin) in BRB80, supplemented with 100 μM Taxol, 6 mM ATP, and an antifade cocktail (120 mM D-glucose, 0.12 mg/ml glucose-oxidase, 0.05 mg/μl catalase, and 0.5% BME) was added to the entrance reservoir. Rhodamine-labeled microtubules were polymerized (37°C for 45 min) from bovine brain tubulin (4 mg/ml, Cytoskeleton, Denver, CO) in a 1:3 stoichiometry of labeled/unlabeled tubulin in the presence of 4 mM $MgCl_2$, 1 mM GTP, and 5% DMSO in BRB80 buffer. Microtubules were stabilized and 20× diluted in BRB80 containing 100 μM paclitaxel.

Electric fields were applied using a Keithley 6517A electrometer. Voltages up to 125 V were applied, where the electrical current would be 2 μA. During experiments, the entrance reservoirs were exposed to atmospheric pressure to prevent a Poiseuille backflow due to EOF-induced pressure build-up. Consequently, the velocity profile in the channel is homogeneous except within the Debye length scale of ≈1 nm from the surface. Joule heating is limited due to the large surface-to-volume ratio of our channels. In steady-state, the electrical dissipation in the channel is balanced by thermal conduction through the glass substrates. For a slit-like channel of height h (filled with a buffer solution of conductivity $\sigma = 1.3$ S/m), the temperature gradient over the glass substrates equals $\frac{dT}{dz} \simeq \frac{\sigma E^2 h}{\lambda}$, where λ is the thermal conductivity of glass (1.4 W/Km). The temperature increase in our channels at the largest field strengths used is thus expected to be limited to ≈1°C with respect to ambient room temperature. An *in situ* probe of the temperature is provided by the velocity of the motility in our channels. Motility speed is known to double for approximately every 10°C increase in temperature (30). The absence of a systematic increase in gliding velocity when an electric field is applied confirms that the temperature increase is limited.

ACKNOWLEDGMENTS. We thank I. Dujovne, T. van der Heijden, J. Kerssemakers, and S. Lemay for useful discussions. We also acknowledge the critical comments of, and resulting discussions with, J. Howard, and an anonymous referee that pointed out the recent theoretical developments concerning the bending mechanics of worm-like bundles. This work was supported by the EC Biomach and the Dutch Organisation for Scientific Research (NWO).

1. Gittes F, Mickey B, Nettleton J, Howard J (1993) *J Cell Biol* 120:923–934.
2. Venier P, Maggs AC, Carlier MF, Pantaloni D (1994) *J Biol Chem* 269:13353–13360.
3. Felgner H, Frank R, Schliwa M (1996) *J Cell Sci* 109:509–516.
4. Kis A, Kasas S, Babic B, Kulik AJ, Benoit W, Briggs GAD, Schonenberger C, Catsicas S, Forro L (2002) *Phys Rev Lett* 89:248101.
5. de Pablo PJ, Schaap IAT, MacKintosh FC, Schmidt CF (2003) *Phys Rev Lett* 91:098101.
6. Janson ME, Dogterom M (2004) *Biophys J* 87:2723–2736.
7. Pampaloni F, Lattanzi G, Jonas A, Surrey T, Frey E, Florin EL (2006) *Proc Natl Acad Sci USA* 103:10248–10253.
8. Bathe M, Heussinger C, Claessens M, Bausch A, Frey E (2006) arxiv.org:q-bio/0607040.
9. Heussinger C, Bathe M, Frey E (2007) *Phys Rev Lett* 99:048101.
10. van den Heuvel MGL, De Graaff MP, Dekker C (2006) *Science* 312:910–914.
11. Cohen AE, Moerner WE (2006) *Proc Natl Acad Sci USA* 103:4362–4365.
12. Riveline D, *et al.* (1998) *Eur. Biophys J* 27:403–408.
13. van den Heuvel MGL, Butcher CT, Lemay SG, Diez S, Dekker C (2005) *Nano Lett* 5:235–241.
14. Kim T, Kao M, Hasselbrink EF, Meyhofer E (2007) *Nano Lett* 7:211–217.
15. Stracke R, Bohm KJ, Wollweber L, Tuszynski JA, Unger E (2002) *Biochem Biophys Res Commun* 293:602–609.
16. Jia LL, Moorjani SG, Jackson TN, Hancock WO (2004) *Biomed Microdevices* 6:67–74.
17. Benetatos P, Frey E (2003) *Phys Rev E* 67:051108.
18. Stigter D, Bustamante C (1998) *Biophys J* 75:1197–1210.
19. Hunt AJ, Howard J (1993) *Proc Natl Acad Sci USA* 90:11653–11657.
20. Kerssemakers J, Howard J, Hess H, Diez S (2006) *Proc Natl Acad Sci USA* 103:15812–15817.
21. van den Heuvel MGL, De Graaff MP, Dekker C (2007) *Proc Natl Acad Sci USA* 104:7770–7775.
22. Duke T, Holy TE, Leibler S (1995) *Phys Rev Lett* 74:330–333.
23. van den Heuvel MGL, Bolhuis S, Dekker C (2007) *Nano Lett* 7:3138–3144.
24. Nitta T, Hess H (2005) *Nano Lett* 5:1337–1342.
25. Clemmens J, Hess H, Howard J, Vogel V (2003) *Langmuir* 19:1738–1744.
26. Hess H, Bachand GD, Vogel V (2004) *Chem Eur J* 10:2110–2116.
27. van den Heuvel MGL, Dekker C (2007) *Science* 317:333–336.
28. Stein D, Kruithof M, Dekker C (2004) *Phys Rev Lett* 93:035901.
29. Coy DL, Wagenbach M, Howard J (1999) *J Biol Chem* 274:3667–3671.
30. Bohm KJ, Stracke R, Baum M, Zieren M, Unger E (2000) *FEBS Lett* 466: 59–62.